DOI: 10.13009/EUCASS2017-340

High-speed and Emission Imaging of a Coaxial Single Element GOX/GCH$_4$ Rocket Combustion Chamber

Fernanda F. Winter†, Simona Silvestri*, Maria Palma Celano*, Gregor Schlieben*, Oskar J. Haidn**
**Technical University of Munich, Chair of Turbomachinery and Flight Propulsion, Division Space Propulsion*
Boltzmannstraße 15, 85748 Garching b. München, Germany
†Corresponding author

Abstract
The start-up process and flame emission has been investigated experimentally using an optically accessible single element combustion chamber operated at 20 bar pressure level. Gaseous methane and gaseous oxygen were injected at ambient temperature with a shear coaxial injector. A high-speed camera was used to detect the flame anchoring near the oxygen post tip. Detection of spontaneous OH* emission has been performed to characterize the flame front and combustion process at different ROFs. In addition, the spontaneous natural flame emission was investigated through the post-processing method of variance to characterize the flame structure and fluctuations.

Nomenclature

ASA	:	American Standards Association
B/W	:	Black and white
CMOS	:	Complementary metal-oxide semiconductor
GOX	:	Gaseous oxygen
GCH4	:	Gaseous methane
LOX	:	Liquid oxygen
NL	:	Natural
OH*	:	Hydroxyl radicals
ROF	:	Oxygen to fuel ratio
VR	:	Velocity ratio
d	:	Diameter
J	:	Momentum flux ratio
$\dot{m}$	:	Mass flow rate
v	:	Velocity
ρ	:	Density

Subscripts

cc	:	Combustion chamber
i	:	Internal
m	:	Methane
o	:	Oxygen
t	:	Total

1. Introduction

Many papers were published in the past years addressing the merits of methane as a propellant candidate. In fact, the propellant combination LOX/methane is a good propellant alternative to the current LOX/hydrogen thrust engines due to its higher density, expected good performance when compared to other hydrocarbons, good cooling capability, low soot production, and low-cost handling [1-4].

DOI: 10.13009/EUCASS2017-340

Although many studies have already been performed [5-7], the development and optimization of a liquid rocket engine for a new propellant combination demand not only detailed understanding of all physical phenomena that determine performance but also validation of numerical tools.
Under these circumstances and considering that the currently established engine concepts depend on a certain number of assumptions due to missing experimental and analytical database, and considering that there is still insufficient knowledge about performance and heat release for this propellant pair, the Technical University of Munich has experimentally and numerically investigated the combustion process and heat transfer of rocket combustion chambers. All combustors operate with gaseous oxygen and gaseous methane in the context of the national research program Transregio SFB/TRR-40 on “Technological Foundations for the Design of Thermally and Mechanically Highly Loaded Components of Future Space Transportation Systems”.
Different numerical tools and approaches have been applied to the single-element combustion chamber with a square cross-section and the results have clearly shown significant differences in their capability to reproduce the experimental heat flux. Although most of the predictions obtain a similar maximum temperature inside the combustion chamber, the predicted flame shapes are different. In general, the predictions vary notably [8].
In order to improve the understanding of the obtained experimental results and to reduce the discrepancies between experimental and numerical results, an optical window has been implemented in the combustion chamber enabling the analyses of test results through optical diagnostics in addition to the classical measurement techniques such as pressure and wall temperature measurements. The optically accessible combustion chamber allows the determination of the flame spreading angle and recirculation length – information which might be relevant for the improvement of numerical tools.
In this context, the present work on flame anchoring and flame emission is performed as a complementation of previous investigations performed on heat transfer [9] and injector-injector/injector-wall interaction [10]. The tests are performed at 20 bar pressure level with mixture ratio variation between 2.2 and 3.4. The images obtained with high-speed and monochrome cameras are used to evaluate the start-up transient phenomena and illustrate not only the global flame structure but also the flame front in the near injector zone.

2. Hardware description

The present test campaign is performed with a modular single-element combustion chamber consisting of two chamber segments, one with 174 mm and another with 145 mm, and one nozzle segment with 20 mm of length. The nozzle has a rectangular cross section of 4.8 mm x 12 mm, as already described in detail by previous papers from Celano et al [11]. The internal combustion chamber dimensions are presented in Table 1.
The combustion chamber used for the tests is capacitively cooled and has a square cross section of 12 mm x 12 mm, see Figure 1. It operates with gaseous oxygen and methane as propellants. The material selected for the combustion chamber and nozzle segments is oxygen-free copper (Cu-HCP) due to its high thermal conductivity. The combustion chamber is equipped with equally spaced pressure transducers and thermocouples type T mounted in the wall along the chamber axis to characterize the combustion process and to monitor heat release.

Table 1: Combustion chamber geometry

Length	290	[mm]
Width	12	[mm]
Height	12	[mm]
Throat height	4.8	[mm]
Contraction Ratio	2.5	[-]

A film cooling system using gaseous nitrogen as coolant is used to protect the quartz window from the heat loads of the combustion. The flat window and the rectangular cross section of the hardware allow optical access to the flame interaction in the near injector area. This setup avoids certain disadvantageous effects, which occur when a flat window is mounted in a round combustion chamber, such as flow disturbances caused by the presence of window corners.
It is assumed that the film cooling mass flow does not influence the near-injector flame stabilization in a significant way. First, because the film cooling mass flow rate is only a small percentage of the total mass flow rate and second, because a non-reactant coolant is used. To confirm these arguments, a sensitivity analysis was performed on a series

DOI: 10.13009/EUCASS2017-340

of tests: No significant difference was observed in the temperature profiles and heat fluxes obtained, therefore the impact of the film cooling was found negligible.
For the current study, a shear coaxial injector element is integrated as shown in Figure 1 with a 4 mm diameter gap for the central oxygen jet and a 0.5 mm annular gap for methane, see Table 2. For simplicity, no tapering or recess is applied.

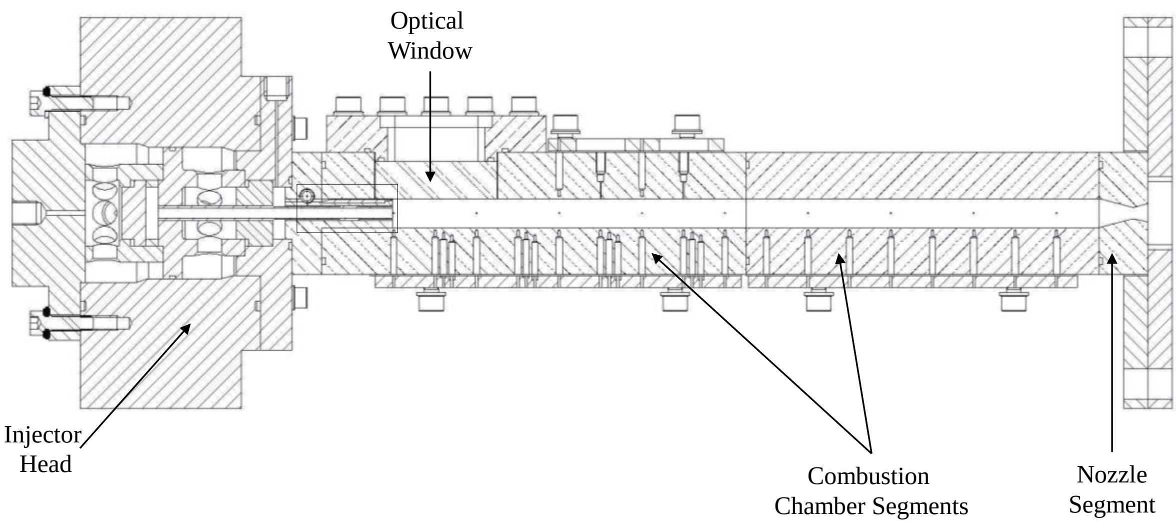

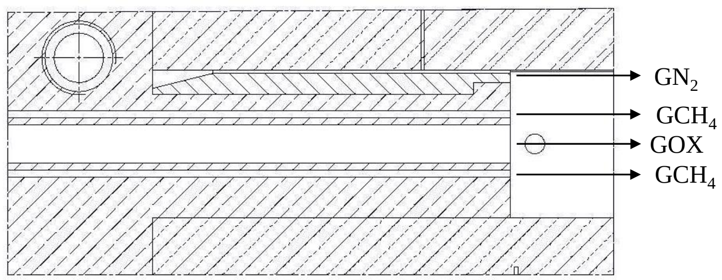

Figure 1: Setup and injector configuration

Table 2: Injector geometry

GOX inner diameter	4	[mm]
GOX post wall thickness	0.5	[mm]
GCH4 external diameter	6	[mm]
Injector area ratio	0.7	[-]

3. Operating Conditions & Sequence

A spark torch igniter is used to ignite the propellant mixture. The igniter operates with gaseous methane and oxygen and is located in the middle of the combustion chamber with respect to the axial direction. Propellants, purge gas, and film cooling mass flow rates can be adjusted by adapting the upstream pressure of sonic measuring orifices located in the feedlines. For determination of the load points, the characteristic velocity is calculated with the software tool NASA CEA2 and combustion efficiency is assumed to be equal to 1. Table 3 summarizes the chosen load points.

DOI: 10.13009/EUCASS2017-340

To operate the combustion chamber, a test sequence is programmed into the control system. As already described and explained in detail in [10, 12], the sequence is divided into three main periods: transient start-up with ignition, main combustion chamber operation and shut down. The igniter operates for 300 ms to ensure ignition of the combustion chamber for a total burning time of 3 s. After successful ignition of the main combustion chamber the igniter is switched off. The same sequence is applied to all of the tests performed.
At first a series of tests was performed at 20 bar pressure level, ROF 2.6 and a film cooling mass flow of 20% with respect to fuel mass flow rate, in order to evaluate the start-up process and flame anchoring. The high-speed camera SpeedCam EoSens mini-2 was used. After these tests, a test campaign was performed at 20 bar pressure level with ROF variation between 2.2 and 3.4 with film cooling percentage reduced to 10% and using the monochrome camera BU205M. The test campaign was performed for two different cases: case A and B. For case A pictures were taken without spectral filter to capture the spontaneous natural (NL) emission of the flame and for case B pictures were taken with a spectral filter combination for emission of hydroxyl radicals. More detailed information about the monochrome camera and the high-speed camera is provided in the next section.

Table 3: Test load points

		ROF [-]				**P_{cc} [bar]**	**$\dot{m}_t$ [kg/s]**	**Film Percentage [%]**
Case A	NL emission	-	2.6	3.0	3.4	20	63.7	10
Case B	OH* emission	2.2	2.6	3.0	3.4	20	63.7	10

4. Optical Diagnostics and Image Processing

The color high-speed camera SpeedCam EoSens mini-2 from HSVision was used to capture the start-up and flame anchoring process. The camera is equipped with an 8-bit CMOS (complementary metal-oxide semiconductor) sensor. The complete optical accessible area is visualized with a resolution of 704 x 480 pixels to a frame rate of 3.000 fps. The camera allows a minimum shutter time of 1 µs and it has a light sensitivity of 400 ASA (American Standards Association).
Figure 2 shows a schematic of the optical setup for two different configurations: high-speed and emission imaging. For the high-speed imaging, the camera was positioned on a tripod next to the test bench and the image of the combustion chamber was reflected into the camera sensor with a planar mirror, which was positioned above the optical window with a 45-degree angle. This setup was chosen to protect this sensitive camera from possible damage.

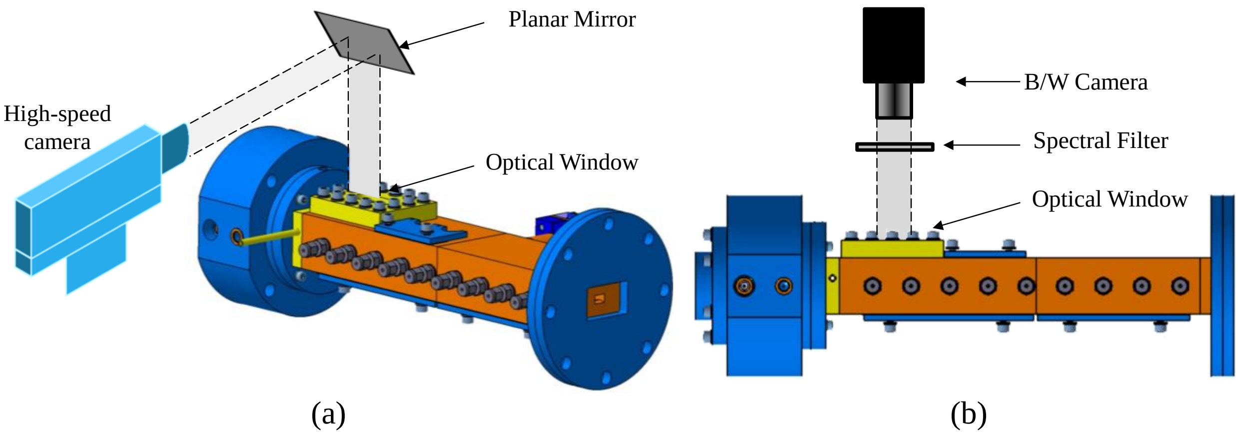

Figure 2: Optical setup for (a) high-speed and (b) emission imaging

DOI: 10.13009/EUCASS2017-340

To detect spontaneous emission of intermittently existing hydroxyl (OH*) radicals and the flame's natural emission, a different camera was selected to record the tests. For the test cases A and B the monochrome BU205M CMOS camera from Toshiba was used. The reason for the selection of this camera is that a monochrome camera has a higher light sensitivity (3800 lx) when compared with color cameras. For the emission imaging, the near-injector area is visualized with a resolution of 2048 x 1088 pixels to a frame rate of 168 fps and shutter time of 50 µs, considering that at high frame rates and lower exposure time, the light intensity is highly reduced.
The camera head was fitted with a 1:1.6 focal length lens and no external lighting was applied. The camera has been set up at the same distance from the combustion chamber to obtain a similar optical resolution for both test cases. For the detection of hydroxyl radical emission, a relevant narrow band-pass filter (308 ± 5 nm) was used. The exposure time of the camera was increased to 5000 µs for case B to obtain a meaningful signal.
The recorded images have been post-processed using image processing tools. Fifty consecutive instantaneous images were averaged in the interval of stable combustion chamber operation. The mean values were then subtracted from each individual instantaneous raw image to calculate the variance of the resulting images. The variance was calculated to have a good overview of the regions of dynamic changes. A contour plot of the average image was created for better visualization of the flame shape. Figure 3 illustrates the image post-processing steps.

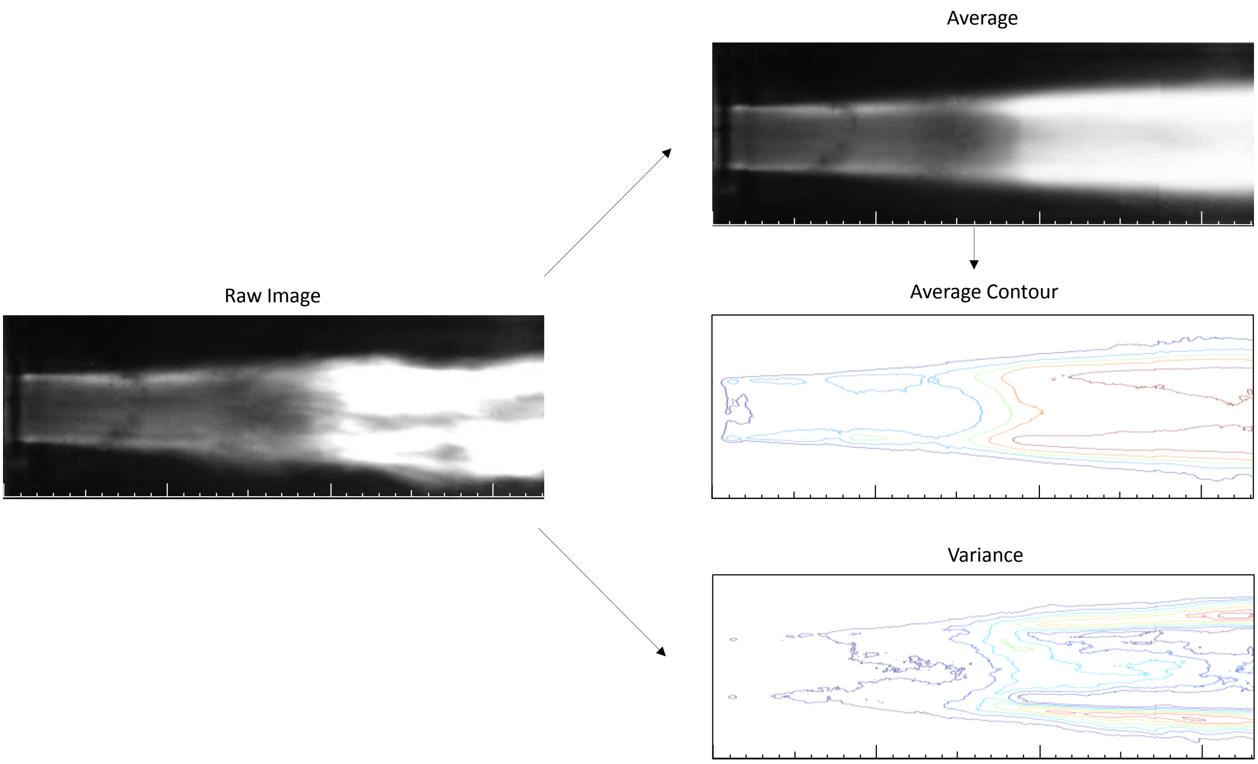

Figure 3: Image post-processing steps

4. Results and Discussion

High-speed imaging was performed on a series of tests at 20 bar pressure and ROF 2.6 in order to detect the start-up process and flame anchoring. Two test cases have been selected for the investigation of the flame emission. In case A spontaneous natural flame emission was detected to illustrate the global flame structure. Since spontaneous emission provides inside information on the process of kinetic chemistry, changes in the burning conditions have an instantaneous effect on emissions and thus on the light that reaches the sensor. In case B the emission of hydroxyl radical have been investigated. As these radicals are formed within the reaction zone, their emission constitutes a signature of the burning conditions. The results are presented in the following paragraphs 4.1 and 4.2.

DOI: 10.13009/EUCASS2017-340

4.1 Start-up

A sequence of acquired pictures of the start-up process until flame anchoring is presented in Figure 4. The edge of the film applicator is visible in the pictures as a reference for the location of the injector. As can be seen in the picture sequence at 0.33 ms, after the igniter is activated in the middle of the combustion chamber the flame moves upstream. The flame then oscillates along the combustion chamber axis at a frequency of about 1 kHz for a time duration of 7 ms. After this initial oscillation, the flame anchors and gets slowly brighter with time. See Figure 5 for a better anchoring visualization. These initial fluctuations in the axial direction occur at a distance not longer than 20 mm from the faceplate.
Due to the high frame rate and small exposure time of the camera, the detected light intensity at the start-up transient process is very low and therefore the flame can be properly detected only after about 100 ms of burning time. An intensifier unit would be necessary for further investigations if the same or higher frame rate would be used. Since intensifier units are very expensive and delicate, it was decided to not only considerably reduce the frame rate but also to use a monochrome camera, which usually has a higher light sensitivity as color cameras, for the emission investigation. The monochrome camera BU205M was then selected for the test campaign. Its light sensitivity is sufficient to capture pictures without and with different spectral filters, allowing in a low-cost way to gather good information of the combustion process with respect to flame structure.

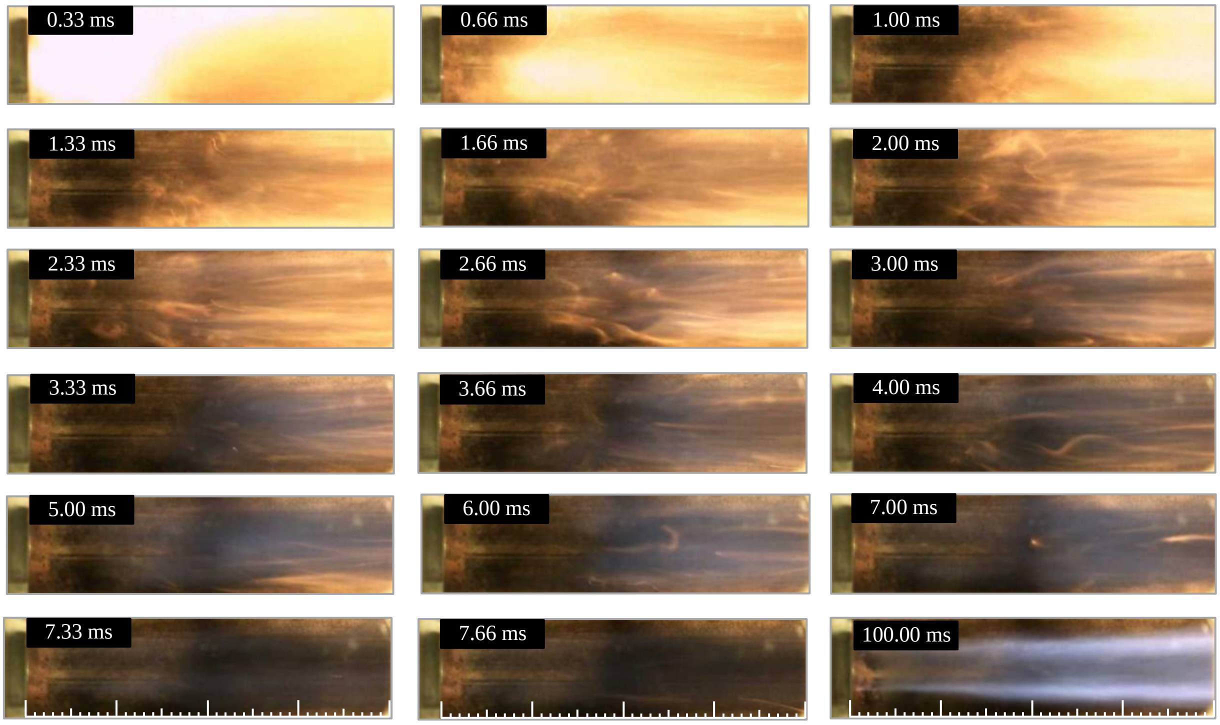

Figure 4: Image sequence of start-up and anchoring

Figure 5: Flame Anchoring

Previous studies [13-15] have already determined that as the flow passes a step, it separates and a shear layer develops, providing a low-velocity zone for the flame to reside and propagate into the reactant flow. This recirculation zone

DOI: 10.13009/EUCASS2017-340

behind the step supplies combustion radicals with enough energy to overcome the activation energy of incoming reactants, thus initiating burning within the shear layer. The flame was attached to the wake of the GOX post-tip for all the tests performed in this investigation.
Another observation from the start-up investigation was that with burning a considerable amount of water was condensing and kept recirculating near the faceplate. In order to suppress condensation of water for the further investigations, the film cooling percentage used to protect the optical window was reduced from 20 to 10% with respect to the fuel mass flow

4.2 Case A

As previously described, case A was dedicated to the investigation of the flame's global structure through detection of the flame's natural emission. For this evaluation, the obtained pictures were post-processed as previously described and illustrated in Figure 3. Figure 6 presents the results of the post-processing. The left side shows the average image of fifty consecutive instantaneous images and its contour for visualization of the flame boundaries.

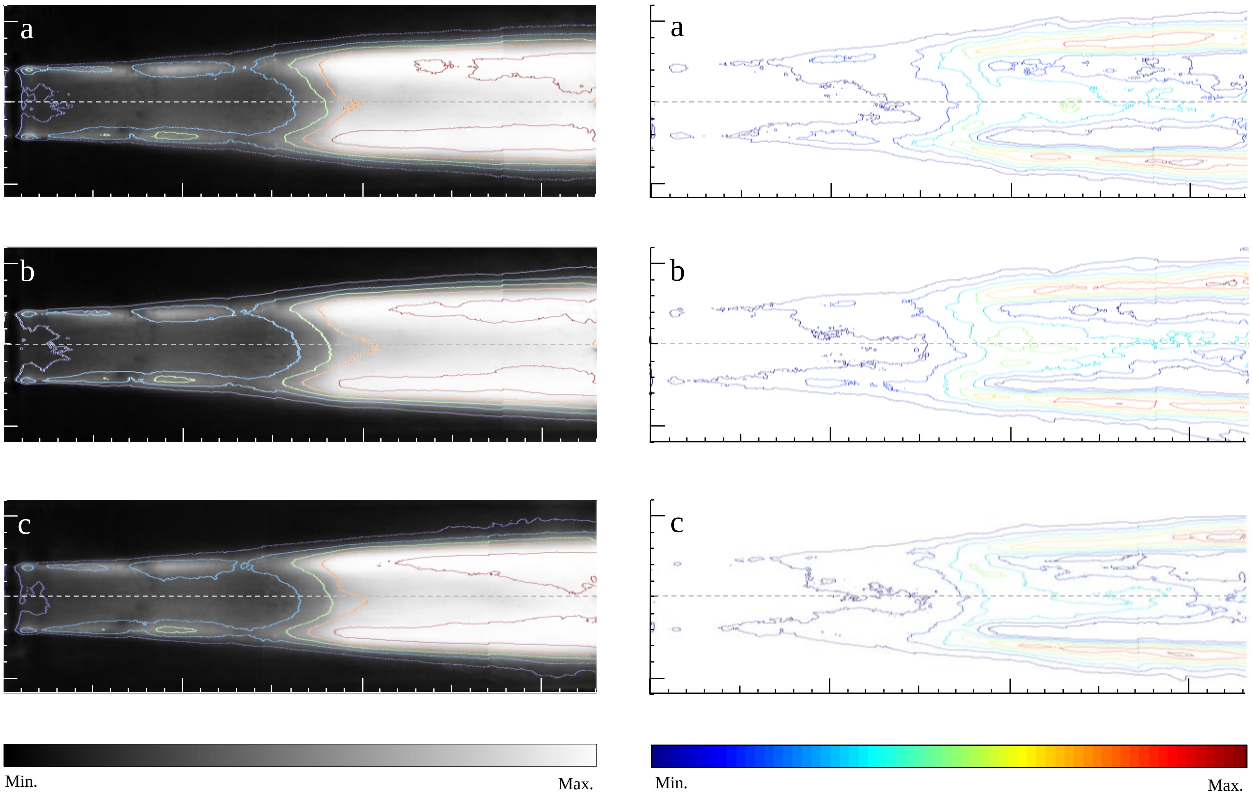

Figure 6: Average contour over-plotted on the average image and variance for ROF (a) 2.6, (b) 3.0 and (c) 3.4 (Scale division: 1mm)

On the right side the correspondent variance is plotted. The variance has been obtained for ROF 2.6, 3.0 and 3.4 to highlight areas of dynamic changes of the flame. As can be seen in the variance images the biggest changes occur at the borders of the flame, due to flame expansion and fluctuations. The flame has a symmetrical shape appearance for all tests performed.
After an axial distance of about 4-5 times the GOX inlet internal diameter d_i, the flame expands radially. The expansion is found to be insensitive to ROF variation, what is in conformance with the tests results reported by Lux et al [16]. The spreading angle in the near injector area is within 4.6° ± 1°. The total flame volume within the optically accessible area seems to not change significantly with ROF, either. Moreover, it seems that for ROF 2.6, for which the external methane jet is faster than the internal oxygen jet, the flame fluctuations are more pronounced when compared to ROF 3.4 and therefore the flame seems slightly thicker. For ROF 3.4, for which the internal oxygen jet is faster, the fluctuations are mainly predominated in the shear layer between the propellants.
The velocity ratio (Eq. 1), momentum flux ratio (Eq. 2) and density ratio, along with other geometric parameters, play an important role in the formation of the shear layer and therefore the spreading angle. This influence is although not

DOI: 10.13009/EUCASS2017-340

more evident, most likely because the velocity difference between the propellants is too low, since the setup operates with a gas/gas propellant pair combination, see Table 4.

Table 4: Characteristic quantities

ROF [-]	v_m [m/s]	VR [-]	J [-]
2.64	146.9	1.10	0.61
3.01	133.8	0.94	0.46
3.36	126.4	0.86	0.37

$$VR = \frac{v_m}{v_o} \tag{1}$$

$$J = \frac{(\rho.v^2)_m}{(\rho.v^2)_o} \tag{2}$$

A certain pattern is observed in all images captured for cases A and B, what is due to soot deposition at the optical window. The pattern has the typical shape of a local recirculation zone and is located at 7 and 15 mm downstream the faceplate. The shape of the deposited soot did not change during the test campaign and therefore it is considered to not have affected the test data.

4.3 Case B

The hydroxyl radical, among other chemical species, is one the most abundant excited radicals produced within the flame front. A typical normalized averaged OH* emission image taken for different ROFs is shown in Figure 7. In all cases the flame is attached and surrounds the gaseous oxygen jet. Other investigations, performed on pre-mixed flames though, have already shown that the OH* emission intensity depends on the equivalence ratio, which is a function of ROF [17]. The images in fact agree with this dependency and indicate that the flame emission is slightly higher for lower ROF.

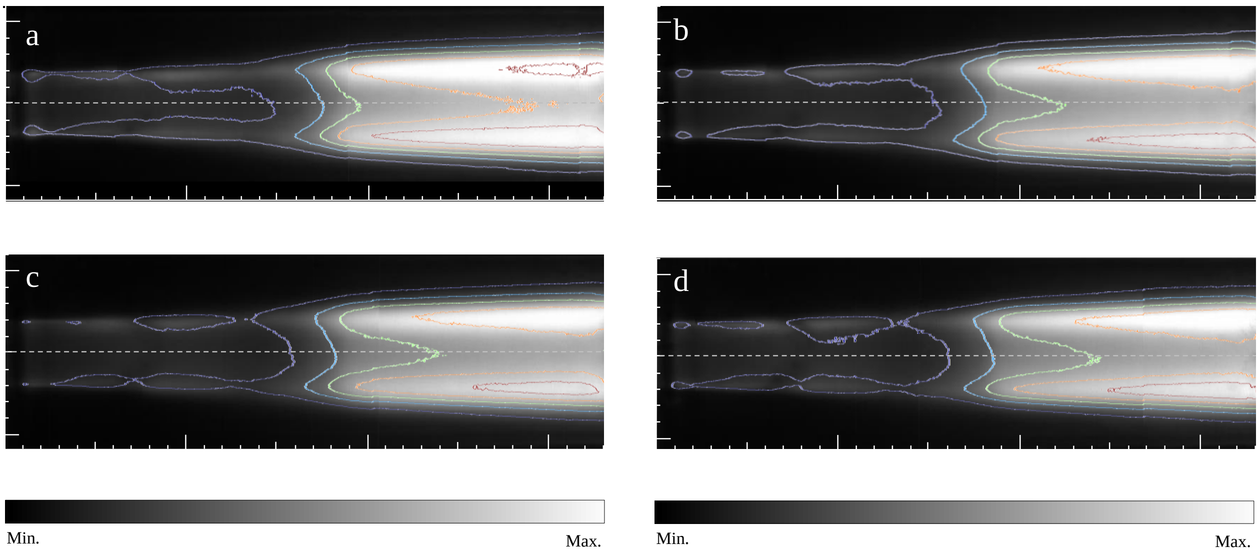

Figure 7: Average picture and average contour for ROF (a) 2.2, (b) 2.6, (c) 3.0 and (d) 3.4

DOI: 10.13009/EUCASS2017-340

In addition, a study on heat transfer [18] in a multi-element rectangular combustion chamber featuring the same geometric parameters and load points ranging from ROF 2.6 to 3.4 has shown that temperature and heat flux for the first 60 mm after the injector faceplate are higher for ROF 2.6 and lower for ROF 3.4. This was physically explained and attributed to the fact that the fuel velocity is lower for ROF 3.4, see Table 4, meaning that the methane jet is pulled inward by the faster oxygen jet, thus increasing the flame front distance to the combustion chamber wall. For ROF 2.6 exactly the opposite occurs and therefore the distance between flame front and combustion chamber wall is reduced.
Interestingly in Figure 7 no significant change in the flame front distance to the combustion chamber wall is observed. Instead it seems that the flame is moved downstream of the faceplate with the increase of ROF what consequently results in lower temperature values and heat flux in the near injector area. According to Perakis et al [18], further downstream where the initial mixing effect is negligible, the energy release increases, the heat flux and temperature values rise and become higher for ROFs, which are closer to the stoichiometric condition.
Although the emission is very low in the centerline of the flame, the emission intensity in all pictures of Figure 7 does not decrease to very low values in that region. That is because emission imaging is a line-of-sight technique and thus light is collected from in front of and behind the focal plane of the camera lens. In future investigations, an Abel transform can be applied in order to compare these experimental results with numerical simulations. Complementary information about the wall heat flux, pressure decay along the combustion chamber axis and temperature profiles obtained from the equally spaced pressure transducers and thermocouples mounted in the wall, can be found in previous publications [9, 11 and 19] or more recently in [20].

Conclusions

High-speed and emission imaging were performed to evaluate the start-up process and to illustrate the global flame structure respectively. For the start-up investigation, a series of tests was performed at 20 bar pressure level and ROF 2.6. Results show that after ignition takes place the flame moves upstream and oscillates along the combustion chamber axis. Anchoring time is of approximately 7 ms and the flame anchors at the wake of the GOX post-tip for all the tests performed.
For the emission imaging two cases were selected. In case A the spontaneous flame natural emission was investigated and in case B the emission of hydroxyl radicals was detected through the use of a bandpass filter. The pictures of the selected cases were post-processed as previously described. In case A the global flame structure and flame fluctuations was evaluated with respect to ROF variation. In case B it was observed that the light intensity is higher for lower ROF and that these results are in accordance with recent studies on heat transfer. Interestingly no substantial difference on the distance from the flame front to the combustion chamber wall was observed for different ROFs, but the flame seems to move in a more downstream position for higher ROF.
It was also observed that the intensity does not decrease to very low values in the center of the flame, because emission imaging is a line-of-sight technique. Therefore, an Abel transform would be necessary for future investigations in order to compare experimental with numerical results.
The emission of other chemical species is also necessary to better understand and interpret the experimental results. For emission sensing to be applied in practical environments, it is necessary to understand the effects of certain parameters, such as pressure, on emission signals, too. Emission imaging is a very useful and fundamental technique in situations where it is technically difficult and/or too costly to apply more sophisticated optical diagnostics.

Acknowledgments

Financial support has been provided by German Research Foundation (Deutsche Forschungsgemeinschaft-DFG) in the framework of the Sonderforschungsbereich Transregio 40. In addition, the authors would like to thank Christoph von Sethe and Mattia Garolli for their support with test preparation and conduction. The authors also greatly acknowledge the help and ideas from Christian Bauer with the image post-processing steps.

References

[1] Haeseler, D.; Bombelli, V.; Vuillermoz, P.; Lo, R.; Marée, T.; Caramelli, F. Green Propellant Propulsion Concepts for Space Transportation and Technology Development Needs. In: *2nd International Conference on Green Propellants for Space Propulsion*, Cagliari, Sardinia, Italy, 7 - 8 June 2004
[2] Vernin, H.; Pempie, P. LOX/CH4 and LOX/H2 Heavy Launch Vehicle Comparison. In: *45th AIAA/ASME/SAE/ASEE Joint Propulsion Conference & Exhibit*, Denver, Colorado, 2-5 August 2009.

DOI: 10.13009/EUCASS2017-340

[3] Burkhardt, H.; Sippel, M.; Herbertz, A.; Klevanski, J. Comparative Study of Kerosene and Methane Propellant Engines for Reusable Liquid Booster Stages. In: *4th International Conference on Launcher Technology " Space Launcher Liquid Propulsion"*, Liège, Belgium, 3 - 6 December 2002.
[4] Pempie, P.; Frohlich, T.; Vernin, H. LOX/Methane and LOX/Kerosene high thrust engine trade-off. In: *37th AIAA/ASME/SAE/ASEE Joint Propulsion*, Salt Lake City, Utah, 8 - 11 July, 2001.
[5] Ueda, S.; Tomita, T.; Onodera, T.; Kano, Y.; Kubota, I.; Munenaga, T. Hot-firing test of methane-fueled rocket engine under high altitude condition. In: *49th AIAA/ASME/SAE/ASEE Joint Propulsion Conference & Exhibit*, San Jose, California, 14-17 July 2013
[6] Lux, J.; Suslov, D.; Bechle, M.; Oschwald, M.; Haidn, O. J. Investigation of sub- and supercritical LOX/Methane injection using optical diagnostics. In: *42nd AIAA/ASME/SAE/ASEE Joint Propulsion Conference & Exhibit*, Sacramento, California, 9 -12 July 2006.
[7] Schuff, R.; Maier, M.; Sindily, O.; Ulrich, C.; Fugger, S. Integrated modelind and analisys for LOX/Methane expander cycle engine. In: *42nd AIAA/ASME/SAE/ASEE Joint Propulsion Conference & Exhibit*, Sacramento, California, 9 -12 July 2006.
[8] Roth, C.; Haidn, O.; Chemnitz, A.; Sattelmayer, T. Numerical Investigation of Flow and Combustion in a Single-Element GCh4/GOX Rocket Combustor. In: *52nd AIAA/SAE/ASEE Joint Propulsion Conference*, Salt Lake City, UT, 25 - 27 June 2016.
[9] Celano, M. P.; Silvestri, S.; Pauw, J.; Perakis, N.; Schily, F.; Suslov, D.; Haidn, O. J. Heat Flux Evaluation Methods for a Single Element Heat-Sink Chamber. In *6th European Conference for Aerospace Sciences*, Kraków, Poland, 29 June - 3 July 2015.
[10] Silvestri, S.; Celano, M. P.; Schlieben, G.; Haidn, O. J. Characterization of a Multi-Injector GOX-GCH4 Combustion Chamber. In *52nd AIAA/SAE/ASEE Joint Propulsion Conference*, Salt Lake City, UT, 25 - 27 June 2016.
[11] Celano, M. P.; Silvestri, S.; Schlieben, G.; Kirchberger, C.; Haidn, O. Injector Characterization for a GOX-GCH4 Single Element Combustion Chamber. In: *5th European Conference for Aeronautics and Space Sciences*, Munich, Germany, 1 - 5 July 2013
[12] Bauer, C. ; Schlieben, G. ; Eiringhaus, D. ; Haidn, O. Design and commission of a mobile GOX/GCH4 rocket combustion test bed for education and collegiate research. *In : Joint Conference 29th ISTS, 24th ISSFD & 6th NSAT*, Japan, 2013
[13] Behrens, A. A.; Lutz, J. M.; Strykowsky, P. J. Instantaneous Flame Anchor Measurements behind a Bluff Body. In: *19th Propulsion Conference*, Costa Mesa, CA, December 2006
[14] Behrens, A. A.; Lutz, J. M.; Strykowsky, P. J. Instantaneous Flame Anchor Measurements behind a Rearward-Facing Step. *AIAA Journal*, v.47, n. 6, June 2009
[15] Frolov, S. M.; Basevich, V. Ya.; Belyaev, A. A. *Mechanism of Turbulent Flame Stabilization on a Bluff Body*. Chem. Phys. Reports, v. 18(8), p. 1495-1516, 2000
[16] Lux, J. ; Haidn, O. Effect of Recess in High-Pressure Liquid Oxygen/Methane Coaxial Injection and Combustion. *Journal of Propulsion and Power*. V. 25, n. 1, January-February 2009.
[17] Guyot, D. ; Guethe, F. ; Schuermans, B. ; Lacarelle, A. ; Paschereit, C. O. CH*/OH* Chemiluminescence reponse of an atmospheric premixed flame under varying operating conditions. *In : Proceedings of ASME Turbo Expo 2010 : Power for Land, Sea and Air*, 14 - 18 June, Glasgow, UK.
[18] Perakis, N. ; Celano, M. P. ; Haidn, O. Heat flux and temperature evaluation in a rectangular multi-element GOX/GCH4 combustion chamber using an inverse heat conduction method. In : *7th European Conference for Aerospace Sciences*, Milan, Italy, 3 - 6 July 2017.
[19] Silvestri, S.; Celano, M. P.; Schlieben, G.; Haidn, O. J.; Knab, O. Comparison of Single Element Rocket Combustion Chambers with Round and Square Cross Section. In *6th European Conference for Aerospace Sciences*, Kraków, Poland, 29 June - 3 July 2015.
[20] Silvestri, S.; Winter, F. F.; Garulli, M.; Celano, M. P.; Schlieben, G.; Haidn, O.; Knab, O. Investigation on Recess Variation of a Shear Coaxial Injector in a GOX-GCH4 Rectangular Combustion Chamber with Optical Access. In: *7th European Conference for Aerospace Sciences*, Milan, Italy, 3 - 6 July 2017.